# Mechanism of Bleomycin Suicide: A Car−Parrinello Molecular Dynamics Investigation

**Anna Karawajczyk,[†] Christian Gossens,[‡] Ursula Roethlisberger,[‡] and Francesco Buda*,[†]**

*Gorlaeus Laboratories, Leiden Institute of Chemistry, P.O. Box 9502, 2300 RA Leiden, The Netherlands, and Laboratory of Computational Chemistry and Biochemistry, Ecole Polytechnique Federale de Lausanne, Federal Institute of Technology, Lausanne CH-1015, Switzerland*

Using first-principles molecular dynamics simulations (Car−Parrinello method) we investigated the possible reaction pathways for decay of the active bleomycin−Fe(III)−OOH complex, so-called bleomycin suicide. The theoretical model of activated bleomycin contains the whole metal bonding domain of the bleomycin ligand. Simulations performed both in a vacuum and in water show that a facile decaying process involves a homolytic O−O bond cleavage with an almost simultaneous hydrogen atom abstraction. The formation of an intra- or intermolecular hydrogen bond appears to be crucial for the decay of the activated bleomycin. We did not observe any evidence of heterolytic cleavage of the O−O bond of the Fe(III)−OOH species.

## 1. Introduction

Bleomycin (BLM) is a six endogenous ligand, which has been used as an antitumor drug (Blenoxane) in the treatment of several types of cancer since the early 1980s.[1] This drug is administered to the patient in the metal-free form. A species called activated bleomycin (ABLM) is formed in the body, and it is identified as a low-spin BLM−Fe(III)-OOH complex by electrospray ionization mass spectrometry (ESI-MS),[2] extended X-ray absorption fine structure (EXAFS) spectroscopy,[3] electron paramagnetic resonance (EPR) spectroscopy,[4] and Mössbauer spectroscopy.[5] The iron atom is coordinated by five nitrogen atoms coming from the bleomycin ligand (the secondary amine of the $\beta$-aminoalanine (A″aALA−N2) segment, the pyrimidine (PYR−N3), the imidazole ring (HIS−I−N5), the amide nitrogen (HIS−A−N4) of the $\beta$-hydroxyhistidine, and the primary amine of the $\beta$-aminoalanine residue (A′aALA−N1) as the axial ligand (Figure 1)) and one end-on peroxide anion (OOH⁻) as the second axial ligand. The activation of oxygen by transition-metal oxides is of fundamental importance in organic synthesis, catalysis, and biochemistry. ABLM is one natural example of such activation similar to cytochrome P450 or methane monooxygenase.[6] The drug acts through peroxide group cleavage that is believed to be the first step driving the DNA double-strand degradation and thus the disruption of the cancer cell. Figure 2 illustrates a well-accepted cycle of BLM activation and deactivation that is broadly discussed in the review paper by R. M. Burger.[1,7] It is interesting that the same products can be formed from DNA when BLM is activated with $Fe^{2+} + O_2$ or $Fe^{3+} + H_2O_2$. That is because both sets of activation cofactors yield the same active state (BLM−Fe(III)−OOH) as is shown in Figure 2. As it appears from the presented cycle, ABLM turns into Fe(III)BLM after causing the oxidative damage of DNA, and the Fe(III)BLM complex can be transformed into Fe(II)BLM and later ABLM in the presence of a reducer and oxygen. This reaction pathway has been verified experimentally

in the Burger group.[8] However, the initial step in the conversion of ABLM into Fe(III)BLM does not appear to necessarily involve DNA, since it occurs both in the presence or absence of DNA.[4] When ABLM decays in the absence of DNA, an irreversible change in BLM occurs. It undergoes a conversion to one or more Fe(III) complexes unable to attack DNA even when aerobic Fe(II) is subsequently added.[8] The reaction is called activated bleomycin suicide because ABLM is a kinetic component in this reaction.[4] The suicide chemistry is very complex,[9] yielding several products[2] and likely involving a modification of the bithiazole moiety.[10]

Studies of the ABLM decay process apart from DNA may provide information about the formation and nature of the BLM intermediate species that may be responsible for the side effects of the drug. However, the characterization of the suicide process may highlight some relevant aspects for DNA degradation by ABLM. One of the most common hypotheses for the initial step in the conversion of ABLM into Fe(III)BLM is a reaction analogous to that observed in cytochrome P450 with a heterolytic O−O bond cleavage[1] leading to a BLM−Fe(V)=O complex as an intermediate state. However, an alternative scenario is a Fenton-like reaction, where the homolytic cleavage of the O−O bond takes place. In this case a hydroxyl radical and an intermediate iron complex BLM−Fe(IV)=O are formed.[11] This Fe(IV)=O complex is much more stable than the Fe(V)=O complex mentioned above as shown by theoretical calculations.[12] The question that we address here is which activation mechanism of the O−O bond plays a role in the self-inactivation of bleomycin. A similar problem is related to the mechanism of action of ABLM on the DNA molecule, but this will not be directly investigated in this work.

Some experimental works concerning the decay of ABLM in the absence of DNA suggest the heterolytic cleavage of the Fe(III)O−OH bond.[13,14] In one of the experimental studies, to clarify the mechanism of the self-deactivation of ABLM, a synthetic model for the metal bonding site of BLM has been treated with Fe(III)−$H_2O_2$ or Fe(II)−$O_2$. A breakdown at the amino acid side chain (N2, Figure 3) of the metal binding site has been demonstrated.[13] Another study for the same purpose but with *N*-[bis(2-pyridylmethyl)aminoethyl]pyridine-2-carboxa-

---

* Author to whom correspondence should be addressed. Fax: +31 71 527 4603. E-mail: f.buda@chem.leidenuniv.nl.
  † Leiden Institute of Chemistry.
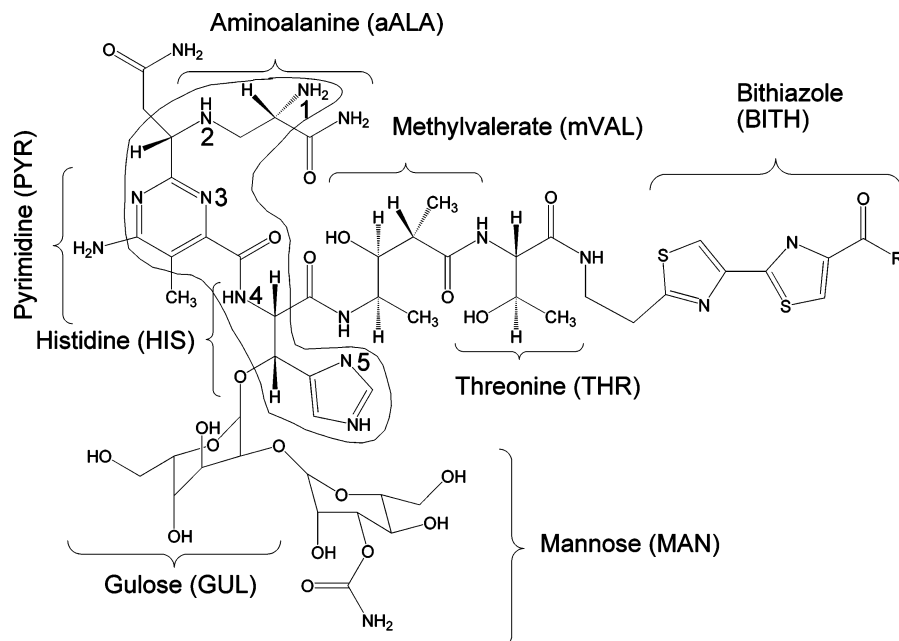  ‡ Ecole Polytechnique Federale de Lausanne, Federal Institute of Technology.

**Figure 1.** Structure of the metal-free bleomycin ligand. The numbers 1−5 indicate the coordination sites to the metal in the activated bleomycin complex. The loop shows the metal bonding domain included in our theoretical model.
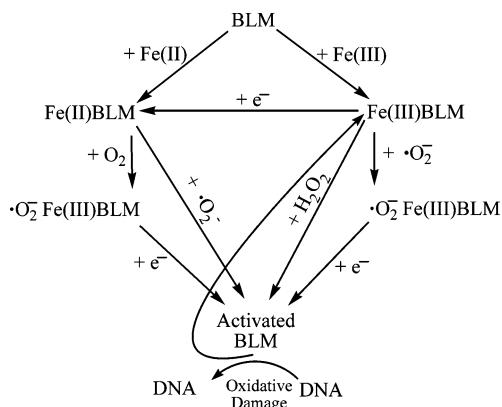


**Figure 2.** Activated bleomycin formation pathways adapted from ref 7. The ABLM can be formed both from Fe(II) and Fe(III) bleomycin complexes. During the degradation of ABLM in the absence or presence of DNA a Fe(III) complex is formed. Formally, the Fe(III)BLM complex can be transformed into Fe(II)BLM and ABLM as shown.



**Figure 3.** Optimized structure of the ABLM model used in this work. The five endogenous ligands of bleomycin (N1, N2, N3, N4, and N5) and the hydroperoxo group (O1, O2, $\alpha = \angle$H−O2−O1, $\beta = \angle$O2−O1−Fe) are explicitly labeled. Additionally, the hydrogen atom $H_{N2}$, which is observed to be abstracted during the CPMD simulations in a vacuum of ABLM, is also marked.

In this paper we present a theoretical investigation of the possible mechanisms of the initial step of the ABLM suicide based on density functional theory (DFT) calculations and Car−Parrinello molecular dynamics (CPMD) simulations. This is the first application of first-principles molecular dynamics to the problem of the mechanism of ABLM self-inactivation, and the choice of this approach is crucial since it allows for an unbiased analysis of the first chemical reaction steps without a predefined reaction pathway.

**2. Model and Computational Methods**

Figure 1 shows a schematic structure of a metal-free BLM ligand. In our model the metal bonding domain is included without any modification. The bithiazole tail and the sugar moiety are neglected as they are not expected to be relevant for our investigation while they are recognized to be important in the process of DNA recognition and binding. Their absence does not modify the coordination sphere of the metal, which is relevant in the process of O−O bond activation. The presence of the bithiazole tail may be important in the next steps of the ABLM suicide, but these are beyond the scope of our present investigation. A realistic model of the coordination sphere of

mide (HPaPy₃) as the ligand modeling BLM demonstrated a modification at the carbon C$\alpha$ to the amide (N1, Figure 3). The modification at this site was suggested to be the result of a two-electron oxidation of the ligand following the heterolytic cleavage of the O−O bond of the Fe(III)−OOH species.[14] However, other evidence from studies performed by Padbury et al.[15] involving the interaction of 10-hydroperoxy-8,12-ocatadecadienoic acid with Fe(II)BLM suggested that the peroxide intermediate of ABLM underwent homolytic O−O bond cleavage to produce the equivalent of a hydroxyl radical and (•OH)−Fe(III)−BLM, which may be the DNA-damaging species. Some other investigators[16,17] in the field showed also that hydroxyl radical can be generated by Fe(II)BLM and proposed that these active radical species may be responsible for degradation of both ABLM and DNA. The Fe(II)−BLM-mediated production of a hydroxyl radical was based on electron spin resonance (ESR) spin-trapping techniques. The existing experimental results are therefore to some extent contradictory and do not provide a clear answer to how the O−O bond is activated in the process of BLM self-destruction.
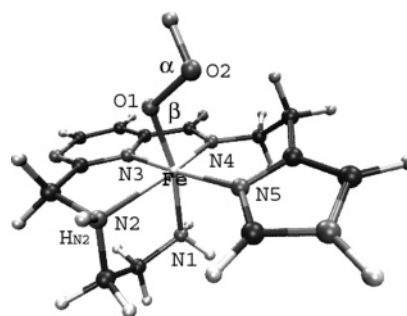
Mechanism of Bleomycin Suicide

*J. Phys. Chem. B, Vol. 110, No. 42, 2006* **21247**

**TABLE 1: Comparison of a Few Selected Parameters (in Å or deg) of the Optimized Geometry of the ABLM Model (Figure 3) with Different Methods[a]**

| | O1−O2 | O2−H | Fe−O1 | Fe−N1 | Fe−N2 | Fe−N3 | Fe−N4 | Fe−N5 | α | β | O1−Fe−N2 | O1−Fe−N5 | H−O1−O2−Fe |
|---|---|---|---|---|---|---|---|---|---|---|---|---|---|
| CPMD/BP | 1.51 | 0.98 | 1.77 | 2.07 | 2.15 | 1.87 | 1.89 | 1.97 | 97.0 | 117.2 | 86.6 | 94.4 | 160.0 |
| ADF/BLYP | 1.48 | 0.97 | 1.78 | 2.09 | 2.17 | 1.89 | 1.91 | 1.99 | 97.9 | 118.0 | 87.2 | 94.4 | 165.7 |
| ADF/BP | 1.46 | 0.98 | 1.77 | 2.07 | 2.15 | 1.89 | 1.89 | 1.97 | 97.4 | 117.2 | 87.0 | 94.3 | 165.8 |
| G03/B3LYP | 1.53 | 0.98 | 1.81 | 2.09 | 2.16 | 1.91 | 1.91 | 1.99 | 98.7 | 116.2 | 86.6 | 94.9 | 157.8 |
| G94/B3LYP[b] | 1.50 | 0.99 | 1.83 | 2.00 | 2.00 | 1.99 | 1.90 | 2.01 | 102.0 | 117.6 | 67.6 | 90.4 | −118.2 |

[a] The CPMD/BP calculations were performed with a 80 Ry cutoff; the ADF/BLYP and ADF/BP were performed with a triple-$\zeta$ basis set with polarization functions, and the Gaussian calculations with the LanL2DZ basis set. [b] The parameters of simplified model used in ref 20. The second axial ligand (N1) and one of the equatorial ligands (N2) are nitrogen atoms of ammonia molecules.

the metal is significant for our study since the reactivity of the Fe(III)−OOH species is strongly dependent on the nature of the metal center ligands. For instance, in the case of the porphyrin ring ligand the reaction of the O−O bond breaking has a heterolytic character, and the ligand stabilizes the peroxidase compound I.[18,19] However, previous CPMD simulations on the $Fe^{III}(H_2O)_5$−OOH complex have shown that the complex is very stable, and no O−O bond cleavage was observed.[11] Static theoretical calculations on the thermodynamics of the O−O bond homolytic cleavage also show that the energy barrier drops from 50 kcal/mol for the $(NH_3)_5$−Fe(III)−OOH complex to approximately 30 kcal/mol for the $(NH_3)_2$(Py)Fe-(III)−OOH complex.[20] Our previous work on the structure determination of Fe(II)BLM[21] also highlights the importance of an accurate model in the theoretical investigation of bleomycin complexes.

The starting structure was based on NMR data for the Co-(III)BLM−OOH complex,[22] with the corresponding Co(III)-to-Fe(III) substitution of the metal center. We have studied our model, which is shown in Figure 3, both in a vacuum and in solution. The calculations in a vacuum allow us to check the stability of the system and to observe the initial step in the ABLM suicide in the absence of any external perturbation or reactant.

The comparison between the simulations in a vacuum and in water enabled us to check the influence of water in stabilizing the O−O bond of ABLM and to check the possible differences in the mechanism of bond cleavage in the initial step of ABLM self-degradation in the gas phase and aqueous environments.

The calculations were carried out using the Car−Parrinello molecular dynamics method [23] as implemented in the CPMD code.[24] The Kohn−Sham orbitals are expanded in a plane wave (PW) basis set with a kinetic energy cutoff of 80 Ry. Our test calculations, which are described in detail in the next section, proved that this cutoff is sufficient for achieving a good convergence of energies and structural properties for the considered systems. We employed ab initio norm-conserving pseudopotentials, generated within the Troullier−Martins scheme.[25] We used a generalized gradient approximation for the exchange−correlation functional, following the prescription of Becke and Perdew (BP).[26,27] All simulations are spin-polarized with a total spin of $S = \frac{1}{2}$. Room-temperature CPMD simulations were performed by using a time step of 0.09 fs and a value of 400 au for the fictitious electronic mass in the Car−Parrinello Lagrangian.

For the simulation in a vacuum we used an isolated cubic supercell of size $17 \times 17 \times 17$ Å$^3$. The simulation in water was performed using a hybrid quantum mechanics/molecular mechanics (QM/MM) approach.[28,29] In particular, the hybrid QM/MM scheme used here is based on the CPMD method for the quantum part and on the Gromos96 MD program[30] for the classical molecular mechanics part. The quantum mechanics part includes the model of ABLM and six water molecules in a cubic

box of $15 \times 15 \times 15$ Å$^3$. The rest of the water molecules were described using the SPC model[31] with the force field implemented in the Gromos96 program. To prepare the initial configuration of ABLM in water we have performed a classical MD simulation using the Gromos96 program, in which the coordinates of the solute molecule were fixed while the 308 water molecules in the box have been relaxed. First, a constant pressure simulation at 300 K and 1 bar was performed for 2 ns, and then a constant volume simulation was performed for 1 ns. After relaxation of the solvent molecules, six waters were found within a distance of 3 Å from the −OOH ligand and have been chosen to be present in the quantum part of the system.

Both simulations in a vacuum and in water start with 1000 steps of relaxation of the system at 100 K. Next the temperature was slowly increased to 300 K.

## 3. Results

**3.1. Test Calculations.** To validate our choice of the density functional, kinetic energy cutoff of PW, and pseudopotentials, we performed a series of test geometry optimizations with different programs using localized basis sets. In particular, we used the Amsterdam density functional (ADF) code,[32] in which the Kohn−Sham orbitals are expanded in a Slater-type orbital basis set, and the Gaussian 03 code[33] using Gaussian-type orbitals. The model of ABLM shown in Figure 3 was optimized by (i) CPMD with a BP functional and a 80 Ry cutoff, (ii) ADF with BLYP and BP functionals with a small core triple-$\zeta$ plus polarization functions basis set, and (iii) Gaussian 03 with a hybrid B3LYP functional and the effective core potential basis set LanL2DZ.[34,35] Moreover, we compared our results to a simplified model of ABLM used in a previous DFT calculation.[20] The results are presented in Table 1. Although all of the relevant geometry parameters are very similar, we noticed that the main differences appear between the parameters describing the simplified model of ABLM from the previous DFT calculations and our model. The Fe−N1 and Fe−N2 bonds lengths in particular are shorter than those in our model as an effect of the presence of two ammonia molecules in the simplified model. That also affects the distance between the iron center and the pyrimidine ring (Fe−N3), which is about 0.1 Å longer in the simplified model, since here the pyrimidine ring is not tightly embedded within the whole ligand structure. There are some dissimilarities between the Fe−O1 bond length computed by Gaussian with the LanL2DZ basis set (~1.82 Å) and the other (~1.77 Å), but more likely that is due to the small basis set in Gaussian/B3LYP calculations. For a proper description of oxygen atoms, a larger basis set is needed.

It has been pointed out recently that not all functionals[36] are appropriate for iron complexes to reproduce the proper ground-state spin polarization. Thus we performed a set of test calculations to verify the accuracy of the BP functional for our systems. In all tested compounds ($Fe^{II}$(BLM)−$O_2$, $S = 0$; $Fe^{IV}$-
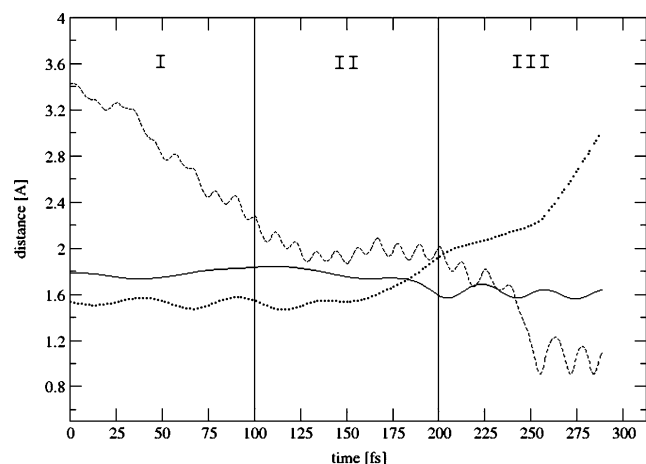
**Figure 4.** Dynamic evolution of a few selected distances along the molecular dynamics of ABLM in a vacuum: (i) full line, Fe−O1; (ii) dashed line, O2−H$_{N2}$; (iii) dotted line, O1−O2.

(BLM)=O, $S = 1$; Fe$^{III}$(BLM)−OOH, $S = ^1/_2$) the calculated ground spin state was in agreement with experimental data present in the literature.[1]

We have also checked the influence of the value of the PW energy cutoff on our system. The test calculations were made for the Fe$^{III}$(NH$_3$)$_5$−OOH complex, HOOH molecule, and OOH anion changing the cutoff value from 70 up to 100 Ry in steps of 10 Ry. The change in the structural parameters when the energy cutoff was increased from 70 to 80 Ry was found to be significant, particularly for the Fe−O and O−O bonds. In particular, with 70 Ry the O−O bond distance was much too long with a value of 1.60 Å in the Fe$^{III}$(NH$_3$)$_5$−OOH complex and 1.56 Å in the OOH$^-$ anion, making the bond weaker and more predisposed to scission. Further increasing the cutoff from 90 to 100 Ry does not change the O−O distance that converges to 1.50 and 1.47 Å for the Fe$^{III}$(NH$_3$)$_5$−OOH complex and the OOH$^-$ anion, respectively. These results justified our choice of computational parameters for the CPMD simulations.

**3.2. ABLM in a Vacuum.** After the initial relaxation of the system we followed the trajectory for a total time of 290 fs at room temperature. In Figure 4 we present the behavior of a few selected bond distances (Fe−O1, O1−O2, O2−H$_{N2}$) along with the dynamics. By analyzing the O2−H$_{N2}$ distance (dashed line), we can distinguish three parts in the dynamics. In the first part (I) the −OOH group is rotating around the Fe−O1 axis. The distance between O2 and the hydrogen atom belonging to the secondary amine of the $\beta$-aminoalanine (A″aALA−N2, indicated in Figure 3) is decreasing, while the O1−O2 bond is stable with an average value of 1.57 Å. After 100 fs the O2 oxygen atom forms a hydrogen bond with the hydrogen atom H$_{N2}$. In the second part of the dynamics (II in Figure 4), we can see that this intramolecular hydrogen bond facilitates the O1−O2 bond cleavage of the hydroperoxo group. After 50 fs from the moment when the hydrogen bond was created, the O1−O2 bond starts increasing from the initial value of 1.58 Å and reaches a value of ~2.00 Å at 200 fs. At the same time the Fe−O1 distance drops to 1.60 Å and oscillates around this shorter value. The just formed OH radical abstracts almost immediately (within 50 fs) the H atom of the secondary amine to form a water molecule. In Figure 4 this fact is illustrated by the oscillation of the O2−H$_{N2}$ bond around a value of 1.00 Å starting from 250 fs. The third part of this MD run (III) illustrates how the formation of the water molecule from the OH radical occurs soon after the O1−O2 bond scission.

We have performed a second CPMD simulation starting from slightly different initial conditions, and we observed the same mechanism for the peroxide cleavage. The only difference observed during the second run was that the system took more time to find a proper configuration to form a hydrogen bond, and because of that the first part of the dynamics was a bit longer (~170 fs). However, the same hydrogen bond was eventually formed with H$_{N2}$, and once this internal hydrogen bond was present, the next steps in the reaction mechanism (II and III of Figure 4) proceeded at about the same speed as in the first run.

To check the energetics of the observed O1−O2 bond cleavage we performed single-point calculations on a few snapshots along the trajectory with O1−O2 distances of 1.47, 1.53, 1.64, 1.88, and 2.05 Å. We observe that the potential energy along this path increases by approximately 12 kcal/mol before decreasing again with the formation of the water molecule. This shows that the thermal energy is enough to overcome an energy barrier of this size. The observed energy maximum corresponds to the snapshot in the trajectory where the hydrogen bond between O2 and H$_{N2}$ is formed ($d_{O1-O2} = 1.64$ Å).

To identify the products of the O−O bond scission we took a snapshot at ~225 fs where the O1−O2 distance is 2.15 Å, and using the ADF program we performed a single-point calculation. The charge on the formed OH species was slightly negative with a value of −0.266 according to the Mulliken analysis, and the spin distribution analysis indicated the localization of −0.5 spin on the oxygen atom of OH species. Therefore we concluded that the OH species can be identified as an OH radical rather than an OH anion.

For comparison, we calculated the energy profile of O1−O2 bond scission in a vacuum at 0 K without the creation of any hydrogen bonds using the geometry obtained for our ABLM model from the Gaussian calculation. The O1−O2 bond was elongated with steps of 0.05 Å from 1.50 to 2.4 Å. The structures were fully optimized with Gaussian 03 as described in the Model and Computational Methods section. We have noticed that the homolytic O1−O2 bond scission is an endothermic reaction with activation energy equal to 17 kcal/mol. The results suggest that the reaction is still possible; however the spontaneous creation of a hydrogen bond observed during molecular dynamics simulations facilitates the scission.

**3.3. ABLM in H$_2$O.** We now investigate the reaction mechanism of the ABLM suicide in water. This simulation will enable us to check the influence of the water solvent on stabilizing the O−O bond of ABLM. After the relaxation procedure, we followed the trajectory for approximately 1 ps. We illustrated the simulation in Figure 5, where the Fe−O1, O1−O2, and O2−H$_{W1}$ distances are plotted. In this simulation we also observed the formation of a hydrogen bond after approximately 500 fs, but in this case the hydrogen bond was formed between the OOH ligand and one of the water molecules indicated as W1 in Figure 6. The following observed reaction steps were similar to those described for the simulation in a vacuum. Simultaneously with the formation of the hydrogen bond, the O1−O2 distance starts increasing (see Figure 5, dotted line at 500 fs). The released OH species remains hydrogen-bonded to W1, and finally after about 400 fs it forms a water molecule by abstraction of a hydrogen atom from the W1 water molecule (see Figure 5, dashed line at ~850 fs). Next we could observe a fast chain reaction where the OH species diffuses through the hydrogen bond network of the water molecules. Figure 6 shows a few snapshots from the dynamics, where this process is well illustrated. In the first panel we show
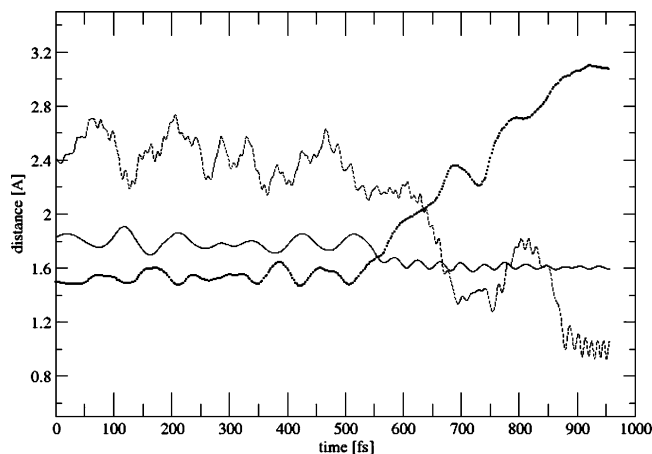
Mechanism of Bleomycin Suicide

*J. Phys. Chem. B, Vol. 110, No. 42, 2006* **21249**

**Figure 5.** Dynamic evolution of a few selected distances along the molecular dynamics of ABLM in water: (i) full line, Fe−O1; (ii) dashed line, O2−$H_{W1}$; (iii) dotted line, O1−O2. $H_{W1}$ is a hydrogen atom from one of the water molecules included in the QM part, indicated also in Figure 6 (W1).
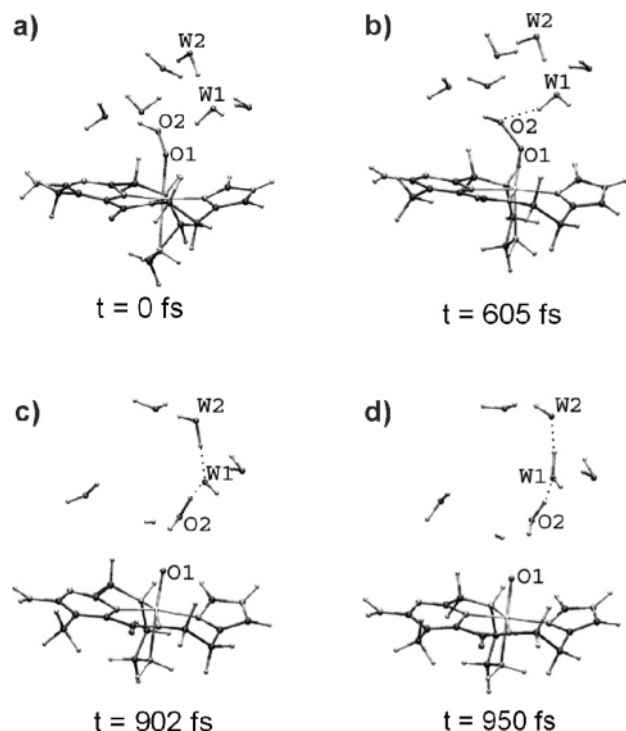
**Figure 6.** A few snapshots along the trajectory of ABLM in water illustrating the relevant steps in the reaction path. Only the quantum mechanics part of the system is shown for clarity. (a) The initial configuration of the system. O1 and O2 indicate the two oxygen atoms of the hydroperoxo ligand; W1 and W2 are the two water molecules that will participate in the diffusion of the hydroxyl radical through the hydrogen bond network. (b) The O2 atom from the OOH group creates a hydrogen bond with the $H_{W1}$ hydrogen atom. (c) The O1−O2 bond is already cleaved, and the $H_{W1}$ is abstracted. The hydroxyl radical (now W1) forms two hydrogen bonds with the newly formed water molecule (O2) and the solvent water W2. (d) The hydroxyl radical moves through the hydrogen bond network of the water solvent (now marked as W2).

the initial configuration at $t = 0$ fs; at $t = 605$ fs we can see the formation of the hydrogen bond with $H_{W1}$; at $t = 902$ fs we observe the breaking of the O1−O2 bond and simultaneous H abstraction and formation of a new water molecule; in the last snapshot we can see the fast propagation of the OH species through the water molecules ($t = 950$ fs) facilitated by the existing hydrogen bond network.

To identify the OH species we performed an ADF single-point calculation for the configuration at 650 fs. As in the case of the vacuum simulations, the OH species was identified as a hydroxyl radical with the spin density localized on the oxygen atom and with a small negative charge. For a complete picture of the observed reaction mechanism and identification of the products, we have also performed a single-point calculation for the same configuration of the system at $t = 650$ fs but with a total spin of $^3/_2$. The total bonding energy was about 10 kcal/mol higher than that for the system with a total spin equal to $^1/_2$. This result shows that no spin flip takes place and our implicit assumption about the conservation of the total spin during the reaction was correct. In the equation below we have also explicitly indicated the total spin of the particles involved to illustrate that the number of unpaired spins can change during the reaction although the total spin is conserved

$$[Fe^{III}(BLM)\text{-}OOH]^+ \rightarrow [Fe^{IV}(BLM)\text{=}O]^+ + OH^\bullet$$
$$\uparrow \qquad\qquad \uparrow\uparrow \qquad\qquad \downarrow$$
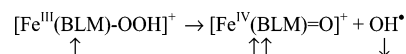
In both single-point calculations with different total spins we observed the spin density localized mostly on the iron atom, on the oxygen atom of the complex, and on the oxygen atom of the OH species. The only difference is that the spin density located on the OH radical is $\beta$-spin for $S = ^1/_2$ while it is $\alpha$-spin for $S = ^3/_2$. We do not see any significant spin density on the equatorial ligands of the iron center, thus ruling out the presence of a cytochrome P450 compound-I-like $[Fe^V(BLM)\text{=}O]^+$ complex. Importantly, this high-valent species, like cytochrome P450 compound I, is better described as a Fe(IV)=O unit magnetically coupled to a ligand radical with the ligand hole essentially localized on the deprotonated amide. A detailed study of the electronic structure of this Fe(V) compound was performed by static DFT calculation in ref 12.

**4. Conclusions and Discussion**

In this work we presented a theoretical study of the mechanism of the first reaction step in the bleomycin suicide based on Car−Parrinello molecular dynamics simulations. We studied an extensive and realistic model of ABLM both in a vacuum and in water solvent. We point out that a proper description of the ligand plays a key role in studying the chemistry of ABLM. Our energy profile for the homolytic O−O bond cleavage calculated in a vacuum gives a reaction energy of 17 kcal/mol, which is about 13 kcal/mol lower than that reported previously.[20] The only difference between these two calculations is in the ligand model. As already mentioned in section 3.1, the previous model was simplified by introducing two ammonia molecules into the coordination sphere of the iron center.

During our simulations in a vacuum and in water we observed hydrogen bond formation prior to O−O bond scission. In a vacuum an intramolecular hydrogen bond is formed between the OOH group and the hydrogen atom belonging to the secondary amine of the $\beta$-aminoalanine ($H_{N2}$), while in the presence of water it is more likely to form an intermolecular hydrogen bond with a water molecule. However, in both cases the formation of the hydrogen bond appears to be a necessary step to facilitate the O−O bond scission by lowering the reaction energy barrier. We have identified the OH species formed in that process as a short-lived hydroxyl radical. This radical immediately abstracts the hydrogen atom participating in the hydrogen bond. The second product of the reaction was identified as the BLM−Fe(IV)=O complex ($S = 1$). Thus we can conclude that in the ABLM suicide process the O−O bond cleavage is homolytic. Furthermore, since the processes of OH

**21250** *J. Phys. Chem. B, Vol. 110, No. 42, 2006*

Karawajczyk et al.

radical formation and H abstraction proceed in a concerted fashion, it is more appropriate to classify the whole mechanism as a direct hydrogen abstraction.

The degradation process of ABLM in the absence of the DNA is rather quick according to our simulations, being observed spontaneously on a picosecond time scale at 300 K. Experimental data give a half-life time of ABLM between 2 min (6 °C, pH = 7.0)[4] or 1.5 min (0 °C, pH = 7.2)[37] and <15 s at pH = 5.8.[37] The experimental results clearly show that the half-life time of ABLM highly depends on the temperature and pH and possibly also other conditions. Even taking into account the somehow higher temperature of our simulations, our reaction rate is definitely much higher than expected. This is likely due to an underestimation of the energy barrier within the approximated exchange−correlation functional used here. It has been suggested that self-interaction corrections (SICs) may improve the accuracy of chemical reactions involving radical species.[38,39] Nevertheless, we think that the mechanism of self-deactivation observed here is realistic although accelerated.

In this first reaction step we observed the formation of two active species that can further react with a substrate, indicating that the whole process of bleomycin suicide is very complex. In the context of the observed homolytic cleavage of the O−O bond, one may easily explain the modification of the bithiazole moiety of bleomycin.[10] Some of the drug side effects may also be associated with the formation of the active species during the degradation process.

A direct hydrogen abstraction was also suggested by static calculations[12] as the most likely mechanism for the radical formation at the C4′ position of the DNA ribose sugar. In fact the reaction with participation of free hydroxyl radical is very unselective, and this is why the direct hydrogen abstraction is much easier to accept. Our study shows that the border between homolytic cleavage and direct hydrogen atom abstraction is very thin. Moreover, we cannot exclude that the Fe(IV)═O complex has a direct role in the DNA attack and is not only an intermediate for regenerating the Fe(III)BLM complex. The BLM−Fe(IV)═O complex seems to be more stable than BLM−Fe(III)−OOH, and it would have a chance to dock to the DNA molecule. However, at this point we cannot make a direct analogy to the reaction of ABLM with DNA, and this issue still requires further investigation.

**References and Notes**

(1) Burger, R. M. *Chem. Rev.* **1998**, *98*, 1153−1169.

(2) Sam, J. W.; Tang, X. J.; Peisach, J. *J. Am. Chem. Soc.* **1994**, *116*, 5250−5256.

(3) Westre, T. E.; Loeb, K. E.; Zaleski, J. M.; Hedman, B.; Hodgson, K. O.; Solomon, E. I. *J. Am. Chem. Soc.* **1995**, *117*, 1309−1313.

(4) Burger, R. M.; Peisach, J.; Horwitz, S. B. *J. Biol. Chem.* **1981**, *256*, 1636−1644.

(5) Burger, R. M.; Kent, T. A.; Horwitz, S. B.; Munck, E.; Peisach, J. *J. Biol. Chem.* **1983**, *258*, 1559−1564.

(6) Solomon, E. I.; Brunold, T. C.; Davis, M. I.; Kemsley, J. N.; Lee, S. K.; Lehnert, N.; Neese, F.; Skulan, A. J.; Yang, Y. S.; Zhou, J. *Chem. Rev.* **2000**, *100*, 235−349.

(7) Burger, R. M. In *Metal-Oxo and Metal-Peroxo Species in Catalytic Oxidations*; Meunier, B., Ed.; Structure and Bonding 97; Springer: Berlin, 2000; pp 287−303.

(8) Burger, R. M.; Peisach, J.; Blumberg, W. E.; Horwitz, S. B. *J. Biol. Chem.* **1979**, *254*, 906−912.

(9) Cheng, C. C.; Goll, J. G.; Neyhart, G. A.; Welch, T. W.; Singh, P.; Thorp, H. H. *J. Am. Chem. Soc.* **1995**, *117*, 2970−2980.

(10) Nakamura, M.; Peisach, J. *J. Antibiot.* **1988**, *41*, 638−647.

(11) Ensing, B.; Buda, F.; Baerends, E. J. *J. Phys. Chem. A* **2003**, *107*, 5722−5731.

(12) Neese, F.; Zaleski, J. M.; Zaleski, K. L.; Solomon, E. I. *J. Am. Chem. Soc.* **2000**, *122*, 11703−11724.

(13) Owa, T.; Sugiyama, T.; Otsuka, M.; Ohno, M.; Maeda, K. *Tetrahedron Lett.* **1990**, *31*, 6063−6066.

(14) Bukowski, M. R.; Zhu, S. R.; Koehntop, K. D.; Brennessel, W. W.; Que, L. *JBIC, J. Biol. Inorg. Chem.* **2004**, *9*, 39−48.

(15) Padbury, G.; Sligar, S. G.; Labeque, R.; Marnett, L. J. *Biochemistry* **1988**, *27*, 7846−7852.

(16) Oberley, L. W.; Buettner, G. R. *FEBS Lett.* **1979**, *97*, 47−49.

(17) Sugiura, Y.; Kikuchi, T. *J. Antibiot.* **1978**, *31*, 1310−1312.

(18) Allentoff, A. J.; Bolton, J.; Wilks, A.; Thompson, J. A.; Demontellano, P. R. O. *J. Am. Chem. Soc.* **1992**, *114*, 9744−9749.

(19) Rodriguez-Lopez, J. N.; Lowe, D. J.; Hernandez-Ruiz, J.; Hiner, A. N. P.; Garcia-Canovas, F.; Thorneley, R. N. F. *J. Am. Chem. Soc.* **2001**, *123*, 11838−11847.

(20) Lehnert, N.; Neese, F.; Ho, R. Y. N.; Que, L.; Solomon, E. I. *J. Am. Chem. Soc.* **2002**, *124*, 10810−10822.

(21) Karawajczyk, A.; Buda, F. *JBIC, J. Biol. Inorg. Chem.* **2005**, *10*, 33−40.

(22) Zhao, C. Q.; Xia, C. W.; Mao, Q. K.; Forsterling, H.; DeRose, E.; Antholine, W. E.; Subczynski, W. K.; Petering, D. H. *J. Inorg. Biochem.* **2002**, *91*, 259−268.

(23) Car, R.; Parrinello, M. *Phys. Rev. Lett.* **1985**, *55*, 2471−2474.

(24) Hutter, J.; Alavi, A.; Deutsch, T.; Bernasconi, M.; Goedecker, S. T.; Marx, D.; Tuckerman, M.; Parrinello, M. *CPMD*, version 3.9; Copyright IBM Corp, 1990−2005, MPI fuer Festkoerperforschung Stuttgart, 1997−2001.

(25) Troullier, N.; Martins, J. L. *Phys. Rev. B* **1991**, *43*, 1993−2006.

(26) Becke, A. D. *J. Chem. Phys.* **1986**, *84*, 4524−4529.

(27) Perdew, J. P. *Phys. Rev. B* **1986**, *33*, 8822−8824.

(28) Laio, A.; VandeVondele, J.; Rothlisberger, U. *J. Phys. Chem. B* **2002**, *106*, 7300−7307.

(29) Laio, A.; VandeVondele, J.; Rothlisberger, U. *J. Chem. Phys.* **2002**, *116*, 6941−6947.

(30) van Gunsteren, W. F.; Billeter, S. R.; Eising, A. A.; Huenenberger, P. H.; Krueger, P.; Mark, A. E.; Scott, W. R. P.; Tironi, I. G. *Biomolecular Simulation: The Gromos96 Manual and User Guide*; Hochschulverlag an der ETH Zurich: Zurich, Switzerland, 1996.

(31) Berendsen, H. J. C.; Postma, G.; van Gunsteren, W. F.; Hermans, J. Interactions models for water in relation to protein hydratation. In *Itermolecular Forces*; Pullman, B., Ed.; D. Reidel Publishing Company: Dordrecht, The Netherlands, 1981; pp 331−342.

(32) te Velde, G.; Bickelhaupt, F. M.; Baerends, E. J.; Fonseca Guerra, C.; van Gisbergen, S. J. A.; Snijders, J. G.; Ziegler, T. *J. Comput. Chem.* **2001**, *22*, 931−967.

(33) Frisch, M. J.; Trucks, G. W.; Schlegel, H. B.; Scuseria, G. E.; Robb, M. A.; Cheeseman, J. R.; Montgomery, J. A., Jr.; Vreven, T.; Kudin, K. N.; Burant, J. C.; Millam, J. M.; Iyengar, S. S.; Tomasi, J.; Barone, V.; Mennucci, B.; Cossi, M.; Scalmani, G.; Rega, N.; Petersson, G. A.; Nakatsuji, H.; Hada, M.; Ehara, M.; Toyota, K.; Fukuda, R.; Hasegawa, J.; Ishida, M.; Nakajima, T.; Honda, Y.; Kitao, O.; Nakai, H.; Klene, M.; Li, X.; Knox, J. E.; Hratchian, H. P.; Cross, J. B.; Bakken, V.; Adamo, C.; Jaramillo, J.; Gomperts, R.; Stratmann, R. E.; Yazyev, O.; Austin, A. J.; Cammi, R.; Pomelli, C.; Ochterski, J. W.; Ayala, P. Y.; Morokuma, K.; Voth, G. A.; Salvador, P.; Dannenberg, J. J.; Zakrzewski, V. G.; Dapprich, S.; Daniels, A. D.; Strain, M. C.; Farkas, O.; Malick, D. K.; Rabuck, A. D.; Raghavachari, K.; Foresman, J. B.; Ortiz, J. V.; Cui, Q.; Baboul, A. G.; Clifford, S.; Cioslowski, J.; Stefanov, B. B.; Liu, G.; Liashenko, A.; Piskorz, P.; Komaromi, I.; Martin, R. L.; Fox, D. J.; Keith, T.; Al-Laham, M. A.; Peng, C. Y.; Nanayakkara, A.; Challacombe, M.; Gill, P. M. W.; Johnson, B.; Chen, W.; Wong, M. W.; Gonzalez, C.; Pople, J. A. *Gaussian 03*, revision C.02; Gaussian, Inc.: Wallingford, CT, 2004.

(34) Hay, P. J.; Wadt, W. R. *J. Chem. Phys.* **1985**, *82*, 270.

(35) Dunning, T. H., Jr.; Hay, P. J. In *Modern Theoretical Chemistry*; Schaefer, H. F., III, Ed.; Plenum Press: New York: 1977; Vol. 3, pp 1−28.

(36) Swart, M.; Groenhof, A. R.; Ehlers, A. W.; Lammertsma, K. *J. Phys. Chem. A* **2004**, *108*, 5479−5483.

(37) Natrajan, A.; Hecht, S. M.; Vandermarel, G. A.; Vanboom, J. H. *J. Am. Chem. Soc.* **1990**, *112*, 3997−4002.

(38) Vydrov, O. A.; Scuseria, G. E. *J. Chem. Phys.* **2006**, *124*, 191101.

(39) VandeVondele, J.; Sprik, M. *Phys. Chem. Chem. Phys.* **2005**, *7*, 1363−1367.